REPORT DOCUMENTATION PAGE

Form Approved
OMB NO. 0704-0188

1. AGENCY USE ONLY (Leave Blank)	2. REPORT DATE	3. REPORT TYPE AND DATES COVERED
	29 March 2002	Final Progress Report Aug. 1, 2000 – Dec. 31, 2001

4. TITLE AND SUBTITLE
Initiation of Chemical Reactions in Energetic Materials Using Plasmas and Arc Channels

5. FUNDING NUMBERS
G
N00014-00-1-0901

6. AUTHOR(S) Mohamed A. Bourham

7. PERFORMING ORGANIZATION NAME(S) AND ADDRESS(ES)
North Carolina State University
Department of Nuclear Engineering
Raleigh, NC 27695-7909

8. PERFORMING ORGANIZATION REPORT NUMBER

9. SPONSORING / MONITORING AGENCY NAME(S) AND ADDRESS(ES)
Office of Naval Research
Ballston Center Tower One
800 North Quincy Street
Arlington, VA 22217-5660

10. SPONSORING / MONITORING AGENCY REPORT NUMBER

11. SUPPLEMENTARY NOTES
The views, opinions and/or findings contained in this report are those of the author(s) and should not be construed as an official Department of the Army position, policy or decision, unless so designated by other documentation.

12 a. DISTRIBUTION / AVAILABILITY STATEMENT
Approved for public release; distribution unlimited.

12 b. DISTRIBUTION CODE

Experiments were conducted to determine the spatial and temporal distribution of the plasma temperature, pressure, number density, and velocity in the plasma-flow-field of an electrothermal source. The experiments revealed a decreasing plasma pressure, plasma temperature and plasma number density as plasma is leaving the capillary source and expands in air. The plasma jet velocity 2 inches from the source exit was found to be about 1300 m/s. Following plasma flow-field characterization, a set of experiment were conducted on the plasma-propellant interaction with increased propellant bed temperature. Experiments were conducted on JA-2 solid propellant with controlled bed temperature. Obtianed results were used to develop a semi-empirical model that includes the bed temperature. Increased burn rates were observed with increased bed temperature, which appears to follow a power $BR = A P^a (T/ T_{ambient})^b$. Further investigation on plasma parameters, through optical emission spectroscopy measurements, allowed modifying the model to include plasma radiative heat flux and plasma number density in the proposed model. Arc channels were initiated in the central perforation of the propellant sample using two arc energy regimes, low and medium energies. The low energy, milli-joule range, has shown weight change of ±0.03 mg. Medium energy range between 260 and 1050 joules has shown an increased weight loss (increased burn rate) with increased arc energy. Experimental data has a linear fit $\Delta m = 2 \times 10^{-4} (E + 282)$, where Δm is the mass loss in mg and E is the arc energy in joules. The linear fit has $R^2 \sim 0.91$. Arc modeling using approximated modified Coulomb logarithm has shown over-prediction of arc plasma parameters, as seen from arc temperature calculated by the model when compared to spectral results.

14. SUBJECT TERMS
Arc Channels, Electrothermal-Chemical Guns, Plasma Ignition, Electrothermal sources, Solid Propellants, Propellant Temperature Sensitivity

15. NUMBER OF PAGES
36

16. PRICE CODE

17. SECURITY CLASSIFICATION OR REPORT	18. SECURITY CLASSIFICATION ON THIS PAGE	19. SECURITY CLASSIFICATION OF ABSTRACT	20. LIMITATION OF ABSTRACT
UNCLASSIFIED	UNCLASSIFIED	UNCLASSIFIED	UL

NSN 7540-01-280-5500

Standard Form 298 (Rev.2-89)
Prescribed by ANSI Std. 239-18
298-102

Enclosure 1

Initiation of Chemical Reactions in Energetic Materials Using Plasmas and Arc Channels

FINAL TECHNICAL REPORT

DR. MOHAMED A. BOURHAM

March 29, 2002

U.S. OFFICE OF NAVAL RESEARCH

CONTRACT N00014-00-1-0901

DEPARTMENT OF NUCLEAR ENGINEERING
NORTH CAROLINA STATE UNIVERSITY
RALEIGH, NC 27695-7909

Acknowledgement

The author greatly acknowledge the US Navy, Office of Naval Research for supporting this research, this work could not have been completed without their support.

The author acknowledges the assistance and help of number of people who worked hard on this project. Mr. Bradford Lambert, a MNE graduate student, who was supported by this contract conducting arc channel experiments and arc modeling; Mr. Ryan Davis, a MNE graduate student, who was also supported by this contract and was the main experimentalist conducting all the experiment on elevated bed temperature; Mr. Brian Bures, a Ph.D. graduate student, who voluntarily helped in many many experimental efforts; Mr. Jeff Preston and Mr. Brian Senter, nuclear engineering undergraduates who provided a lot of experimental preparations and helping running the experimental facility.

Table of Contents

Abstract

Previous experiments on plasma-propellant interaction have shown enhanced burn rates. The temperature of the propellant's bed may play a role in the burn rates under plasma injection. In this report, a set of experiments were first conducted on the plasma-flow-field to determine the spatial and temporal distribution of the plasma temperature, pressure, number density, and velocity. The experiments revealed a decreasing plasma pressure, plasma temperature and plasma number density as plasma is leaving the capillary source and expands in air. The plasma jet velocity 2 inches from the source exit was found to be about 1300 m/s. Following characterization of the plasma-flow-field, a set of experiments were conducted on JA-2 solid propellant with controlled bed temperature. Experiments, with proposed models, revealed a functional form that includes the bed temperature. Increased burn rates were observed with increased bed temperature, which appears to follow a power law. A model for the burn rate is proposed, which includes the bed temperature and has the $BR = A\, P^{a} \left(T / T_{ambient} \right)^{b}$. Further investigation on plasma parameters helped in modifying the model to include plasma radiative heat flux and plasma number density in the proposed model.

I. Introduction

Electrothermal plasma has been studied as a viable replacement for solid propellant ignition. The studies were not only conducted for possible ignition using plasmas, but also as means of controlling and enhancing burn rates of propellants. With plasma augmenting the propellant's burn rate, a mix between plasma electrical energy and chemical energy of the propellant may provide a possible means of achieving high enthalpy flows. Such high-enthalpy flows may provide better interior ballistics and higher muzzle velocities for hyper-velocity launchers [1-8]. Previous work has shown that the plasma ignited propellant burn increases surface erosion compared to that of conventional ignition [1-5]. Those experiments studied the effects of plasma pressure impact on the burn rate of propellant when the propellant was at ambient conditions. No propellant bed temperature sensitivity has been examined, as of yet, when the propellant is ignited by electrothermal plasmas.

This work will determine if any propellant temperature dependence exists in the burn rate and, if it exists, the functional form of that dependence. A series of experiments was performed on NCSU's PIPE [2,4,5, 9,10] ETC device that impacted plasma onto a heated propellant bed (JA2). Experiments were conducted using an incomplete "extinguished" burn technique to provide an evaluation of the erosive burn. These plasma impacts resulted in propellant mass loss that could be correlated to burn rate. If propellant bed temperature significantly impacts the burn rate of the propellant then this would be shown in the experimental data returned from the mass loss as compared to burn rates at ambient temperature. The experiments also required a pressure difference so the propellant was placed at 1, 2 and 3 inches from the barrel. This allowed for a correlation based on pressure and propellant bed temperature. Additionally, the radiative heating effect of the plasma on the propellant bed could be evaluated from the plasma temperature change farther away from the barrel.

The main goal of the work is to determine a functional equation that can be used with common diagnostics to determine the impact of the bed's temperature on burn rates. Pressure is commonly measured in expansion chambers and is relatively easy to obtain. As a result, the functional form will have pressure and bed temperature dependence and the burn rate with these dependencies can be calculated. The final goal of all current propellant studies is the development of a plasma-sensitive propellant that will only combust when burned with plasma. This will be a safer propellant that will not

combust under fire or by any other accidental means. This work continues the efforts to develop such a plasma sensitive propellant for the viable use of ETC launchers.

Many researchers have studied, in detail, the interaction of plasma with propellants. Electrothermal plasmas are used because they are characterized by their high-density and relatively low-temperature (1-10eV) such that ET plasma resembles a blackbody [7-16].

The majority of the research at the ARL has been performed in order to determine the effects of plasma temperature, pressure, and radiation effect [16-21]. In general, these are compared with the conventional black powder ignition means in a large assembly that simulates how a full propellant packed charge would burn. These provide a good indication of how a real cannon device would be operated and an idea of the geometry of the burn propagating through. However, these closed bomb devices don't lend themselves well to the study of optimization because of the burning and pressure due to other grains. Individual grain study is useful for determining the actual effect of plasma on the propellant and gives an idea as to the improvements in packing geometry or even chemical composition to give the desired burn characteristics. NCSU's plasma engineering group has ETC devices that are ideally suited for single propellant grain plasma experiments and as a result are contracted by ARL to perform propellant studies.
Previous work has shown geometry effects by rotating the propellant to change the plasma impact angle. The study revealed that normal impact results in the highest burn rate.

The traditional form of the combustion equation comes from chemical kinetics. For example a bimolecular reaction of the type

$$A + B \rightarrow M + N$$

The rate of reaction is proportional to the probability of collision in the molecules. This probability is determined by the number of moles per unit volume or the concentrations. Hence

$$-\frac{dN_A}{dt} = -\frac{d(VC_A)}{dt} = -\frac{dN_B}{dt} = -\frac{d(VC_B)}{dt} = kVC_AC_B$$

where V is the volume and k is the reaction rate constant.

Performing differentiation and dividing through by a constant volume yields

$$-\frac{dC_A}{dt} = -\frac{dC_B}{dt} = kC_AC_B$$

If the reaction proceeds as the stoichiometric equation states

$$aA + bB \rightarrow mM + nN$$

then the rate of change of the concentration is related to those remaining and can be written in the form [22]

$$-\frac{dC_A}{dt} = k_n C_A^n$$

The concentration can be written as density times the mole fraction and taking the full derivative of the concentration yields

$$-k(\rho\varepsilon)^n = \rho\frac{\partial\varepsilon}{\partial t} + \varepsilon\frac{\partial\rho}{\partial t}$$

Dividing by a constant density and solving for the change in mole fraction gives

$$\frac{\partial\varepsilon}{\partial t} = -k\rho^{n-1}\varepsilon^n$$

The mole fraction lost due to combustion is proportional to the burn depth of the material and density times the mole fraction is proportional to pressure. This allows the equation to be written in the conventional form of the Saint Roberts Equation [5]:

$$BR = bP^{\alpha}$$

with P in psi where α takes care of the combination of n and n-1. The value for the exponent n was determined experimentally for the modified double base propellant JA2 to be n=1.3755. The b was determined to be $8.865\text{x}10^{-5}$. This value is higher for plasma impacted propellant than for the conventional black powder combustion n=0.889 and b=$203.2\text{x}10^{-5}$ [4]. This results in higher burn rates for an equivalent pressure (because the value of b is constant for each propellant) which would change the ballistics of a projectile launched by the propellant (and is necessary to know in the case of cannons). Bourham also showed experimentally that the burn rate is not dependent solely on pressure but is also coupled with the radiation heat flux from the plasma temperature. This was done by comparing effects of single and double exposed samples [4]. The samples that were exposed twice, once on each face of the propellant, showed a higher gasification rate. The conclusion was drawn that this gasification rate was due to the in-depth reactions caused by the radiation flux of the plasma.

It has also been shown that the only augmentation the plasma gives to the propellant burn rate is during the actual plasma impact and there are no secondary burn rate augmentations. This was shown by Birk [8] who also did some experiments with chilled propellants. His results with the M30 propellant showed that the burn rate at –22 C was significantly lower than those samples exposed at 22 C. Even though he didn't have any comparative data for the JA2 propellant, one can conclude that a similar effect should take place with the JA2 propellant.

If this temperature effect had a considerable impact on the burn rate of a propellant, then this effect must be quantified. The artillery officer in charge of the weapon and fire guidance must know how the environment is going to impact the range and the exterior ballistics. If the weapon is deployed into an environment similar to Siberia or to an environment like the Sahara Desert the artillery officer may not have time to calibrate the devices using a trial and error method.

Information about the firing of the propellant should be available in order to determine if the environment will affect the firing and to what extent the environment will impact the propellant.

For this reason, it is proposed to modify the burn rate equation to include propellant bed temperature dependence in the form

$$BR(P,T) = aP^b f(T)$$

All of the previous experiments to determine the constant a and exponent b were done at an ambient temperature assumed to be 20 °C, but the propellant temperature was not monitored. This work will determine if the propellant temperature does have a significant impact on the burn rate of plasma ignited propellant and if so, what the pressure-temperature dependent burn rate would be. It is assumed that the burn rate dependence on pressure will remain as a power law but it is possible that the temperature dependence could follow a power or an exponential form

$$BR = aP^b T^c$$

or

$$BR = aP^b \exp(cT)$$

The bed temperature may also be expressed as a ratio between the raised temperature and the temperature at ambient:

$$BR = aP^b \left(\frac{T}{T_o}\right)^c$$

where T_o is the ambient temperature.

The expectation is that there will be propellant temperature sensitivity in the burn rate. Beyer [7] already showed some effect of cooling of M30 propellant and this side note found in his work must be expanded on. However, it makes sense logically that the temperature of the propellant bed would have an effect on burn rate because as the temperature changes in the bed, so does the energy of the bed. Molecules that are excited are more likely to dissociate from each other when ignited, thus increasing the burn rate.

II. Plasma Flow-Field Characterization

Plasma flow-field characterization and distribution of plasma parameters, both spatial and temporal, gives an accurate picture on the environment where the propellant bed is placed within during exposure to electrothermal plasma. With controlled bed's temperature to evaluate the sensitivity of the propellant to the plasma jet at elevated temperatures, it is necessary to determine the plasma parameters in the plasma-flow field. Plasma pressure and temperature of the plasma jet outside the electrothermal source must be known by direct measurements. These measurements can help determining the momentum and energy terms at any chosen location, and thus the plasma impact on the propellant bed can be expressed in terms of the plasma parameters at chosen location. Before conducting temperature sensitivity studies, the plasma-flow-field experiments were conducted and the pressure, temperature, density and velocity

distribution in the flow-field were measured. A compact multi-sensor probe has been designed and constructed to measure spatial and temporal plasma parameters. These parameters are the total and Static plasma pressure, plasma temperature, plasma number density and plasma Velocity. All measurements were conducted at atmospheric pressure by fusing the ET source with aluminum fuses. The ET plasma is thus jetting into open air inside of a cubical chamber. The plasma jet expands out of the ET source with a measured expansion angle of approximately 23° from the ET source's axis.

II.1 The Compact Multi-Sensor Probe:

The compact multi-sensor probe [23], as shown in the Fig. 1 below, has two absolute pressure transducers (Kistler Model 601B) and three fiber optic cables. The sensor head is arranged such that the two pressure transducers are close to each other with one pointing towards incoming plasma flow to measure total pressure, and one situated upright to measure the static pressure.

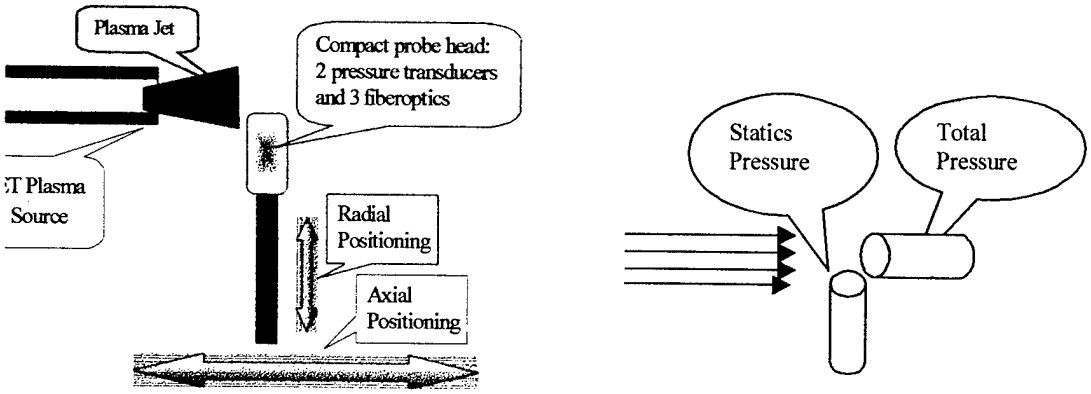

Fig. 1 Schematic of the concept of multi-sensor probe equipped with two pressure transducers and three fiber optic cables. Positioning of the pressure transducers is shown at right.

To calibrate the pressure transducers, a shock tube was designed, constructed and used for calibration. It consists of a high-pressure chamber and a barrel section, separated by a burst disc. The high-pressure chamber is connected to a compressed nitrogen cylinder and set to the desired pressure. The valve is shut and the device is triggered abruptly via a plunger, which in turn forces the burst disk to burst and thus forwarding a shock wave down the test barrel. Pressure signals are recorder on a LeCroy 9310 digital storage oscilloscope. It was determined that the relation between the true pressure versus measured pressure is linear and is expressed by $P_{true} = 1.03\ P_{measured} - 0.46$. The three fiber optic cables are arranged as a bundle, with one fiber optic interfaced to an optical multichannel analyzer for time-integrated optical emission spectra measurements, and two other fiber-optics each is interfaced to a monochromator and a photomultiplier for time-resolved spectral measurements. Monochromators were adjusted to 521.82 nm and 570.02 nm wavelengths (copper lines). Optical emission spectroscopy [24-26] was used to measure the plasma temperature, assuming plasma is at LTE, and plasma-density from optical lines broadening. Three axial locations were chosen for measurements, 2.4, 3.4 and 4.4 inch from source exit. At each axial location, three radial locations are defined to measure distributions within the diverging plasma jet. Figure 2 bellow shows the source exit and the locations of compact multi-sensor probe measuring positions.

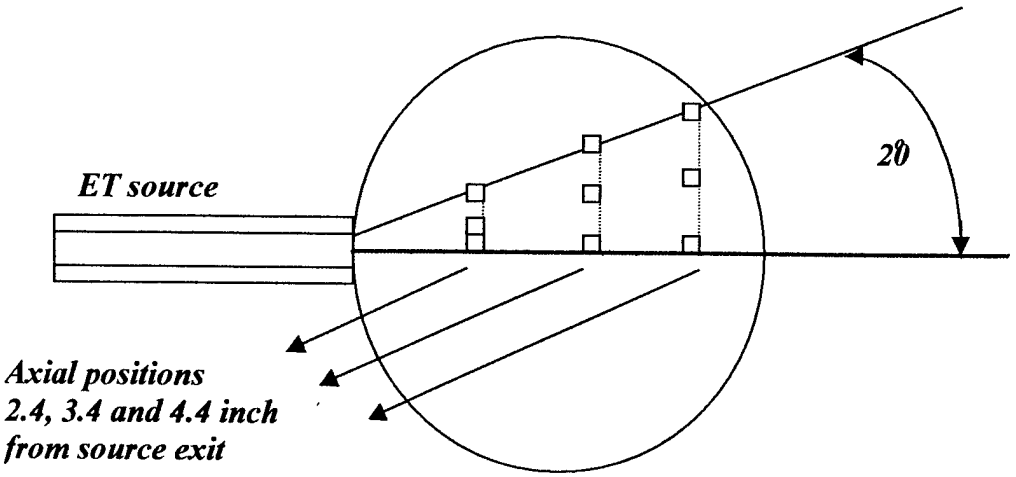

Fig. 2 Schematic showing selected locations to obtain spatial distribution of electrothermal plasma parameters down stream from the source exit and within a 20° angle.

Selection of the measuring locations is based on the plasma jet divergence as the plasma leaves the source. The angle was measured by placing a witness plate in the plasma stream along the axis of the device. The nine selected location covers the solid angle of divergence and provides a detailed information on the spatial distribution of the plasma jet parameters.

II.2 Plasma-Flow-Field Distribution:

Plasma parameters at 2.4, 3.4 and 4.4 inches from the source exit were measured, and at three radial locations for each axial position. Figures 3 and 4 show the pressure distribution from the source exit. Figure 3 shows the results of the peak total pressure, where it is obvious that the axial profile is approximately flat for all radial locations, while the radial profiles are of a top-hat distribution. The measurements imply that for axial locations between 2 and 4 inches, the plasma jet undergoes an essentially isentropic expansion, while the edge of the jet is subjected to mixing process with the surrounding gas.

Figure 4 shows the distribution of the peak static pressure, where the general trend indicates a decrease in the static pressure as the jet expands. Of course the largest static pressure is at the location closest to the source exit.

Of importance is the distribution of the plasma temperature and density. The spatial distribution of the plasma temperature is shown in Fig. 5. These temperatures were obtained from time-integrated optical emission spectroscopy using copper lines. The plasma temperature drops quickly from 2.1 eV right at the source exit (axial distance = 0) to approximately 0.5 eV at 2 inches down stream. Further into the stream, one may observe that the plasma jet is approximately isothermal. With additional data from time-resolved spectral measurements of copper lines, it was obvious that the plasma temperature inside the jet is 0.4 +/- 0.16 eV. A slight increase in the plasma temperature was observed at 4.4 inches from the source exit. Such temperature increase is attributed to the expansion of the plasma jet.

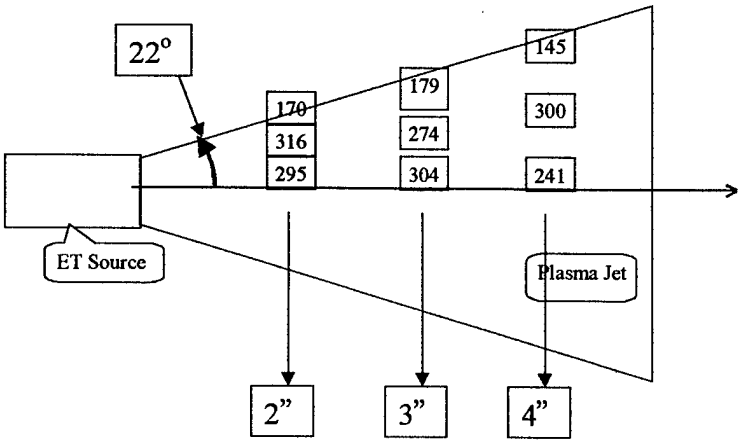

Spatial distribution of peak total pressure (psig) of the plasma jet as measured from the source exit

Fig. 3 Peak total pressure in the expanding plasma jet

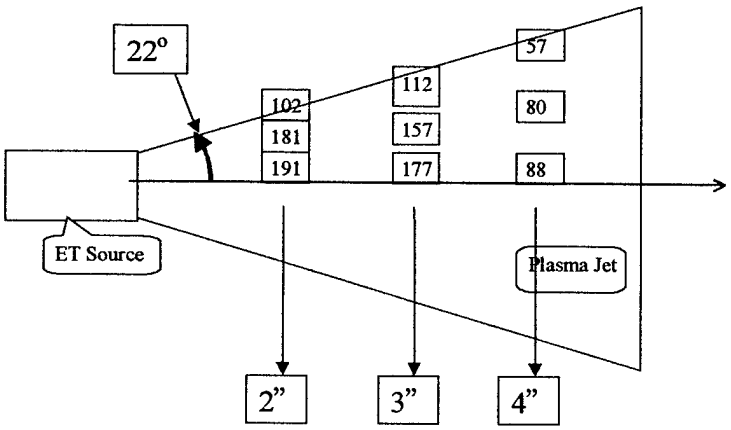

Spatial distribution of the peak static pressure (psig) of the plasma jet as measured from the source exit

Fig. 4 Peak static pressure in the expanding plasma jet

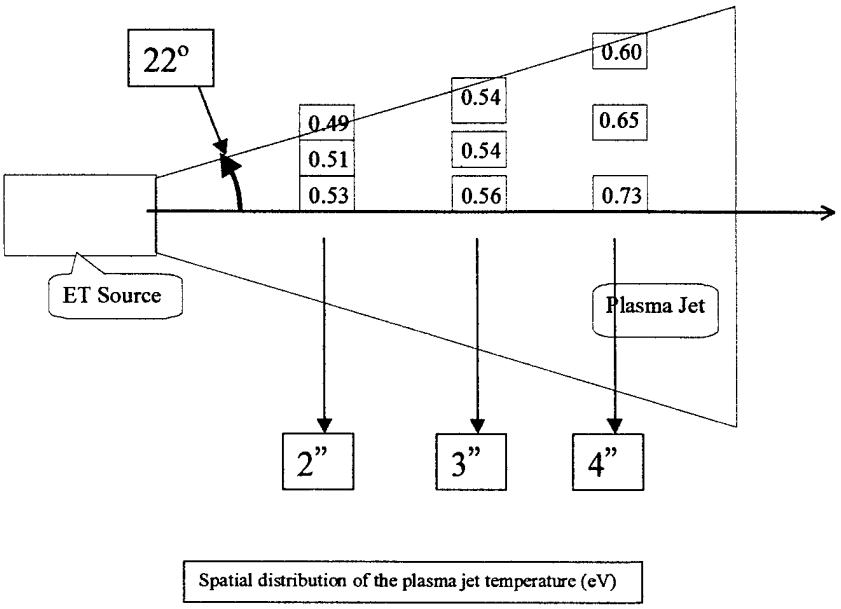

Fig. 5 Average plasma temperature in the expanding jet

The plasma density is another important parameter. It was calculated from the peak static pressure and the time-integrated plasma temperature. The plasma density at spatial locations of measured pressure and temperature is shown in Fig. 6. The density decreases with increased axial length as well as increased radial position. This is expected for an expanding plasma jet from an electrothermal source. It is obvious that the plasma density follows the static pressure distribution, especially that the temperature is almost same inside the jet and thus the density profile follows the static pressure profile.

The average speed of the plasma jet was obtained from the plasma arrival time to the sensors at the chosen measuring locations. The speed of the jet is approximately constant and close to 1300 m/s on axis. The slowing of the plasma near the jet boundary is attributed to the mixing processes with the surrounding air. For a 0.5 eV ideal gas, the sound speed is 3100 m/s, and thus the measured speed indicates that the jet flow is sub-sonic with a Mach number of about 0.4. The time-resolved spectral measurements were also used to calculate the plasma precursor, from which the precursor plasma velocity is found to be about 3000 m/s. Fig. 7 shows the average plasma speed in the expanding jet.

The obtained parameters are important in deciding where to place the propellant for a given experiment, and what to be expected in terms of plasma parameters, at any selected location.

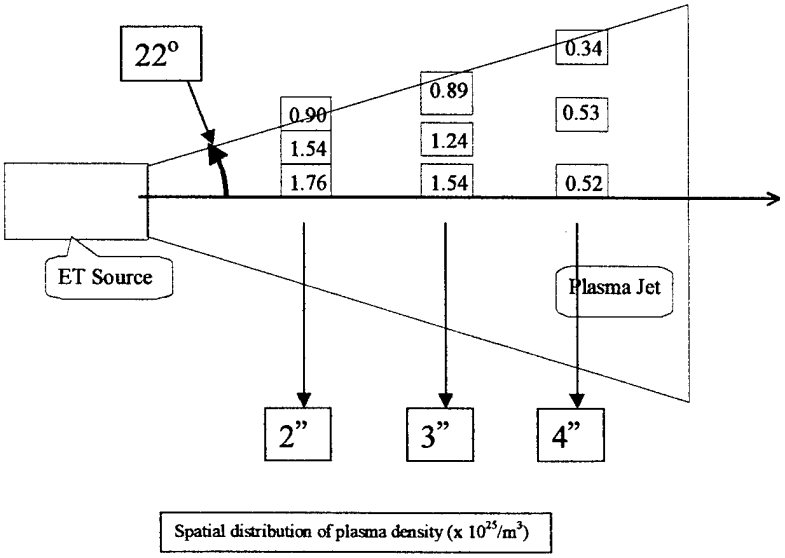

Fig. 6 Plasma density distribution in the expanding jet

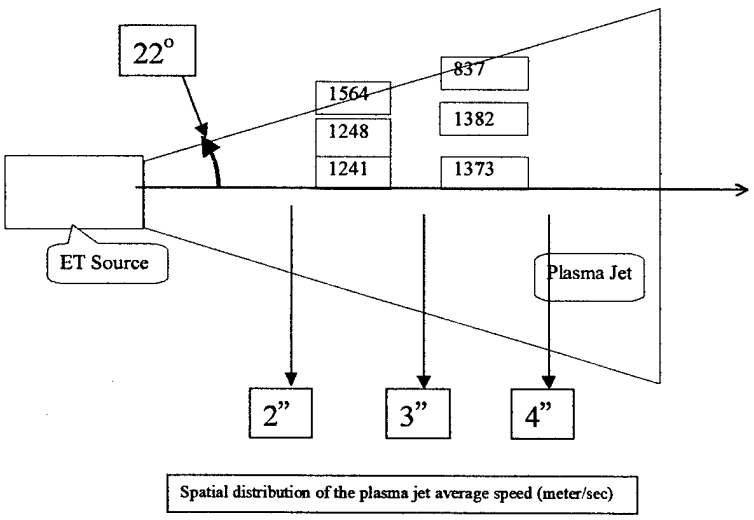

Fig. 7 Average plasma speed in the expanding jet

III. Temperature Sensitivity Studies

Temperature sensitivity of the propellant bed may alter the burn rates under plasma injection. When the bed's temperature is elevated, it is expected that the burn rates would increase as a result of increased in-depth heating of the bed. Also, the plasticizer may migrate causing alterations in the burn rates. A temperature-control unit is designed such that the bed's temperature prior to plasma injection is maintained constant. The bed temperature can be elevated up to 100°C , however, the upper limit was set to 50°C [27].

III.1 Experimental Arrangement:

A circulating cooling unit was designed, constructed and tested for operation. Preliminary experiments on the circulating cooling control unit have shown the necessity of long time circulation of the fluid in order to maintain temperature stability. A modified design using heating elements allowed for a faster temperature setting prior to plasma injection. Figure 8 shows the experimental arrangement using heating elements to fulfill the temperature sensitivity studies with elevated temperatures between 20 to 50°C.

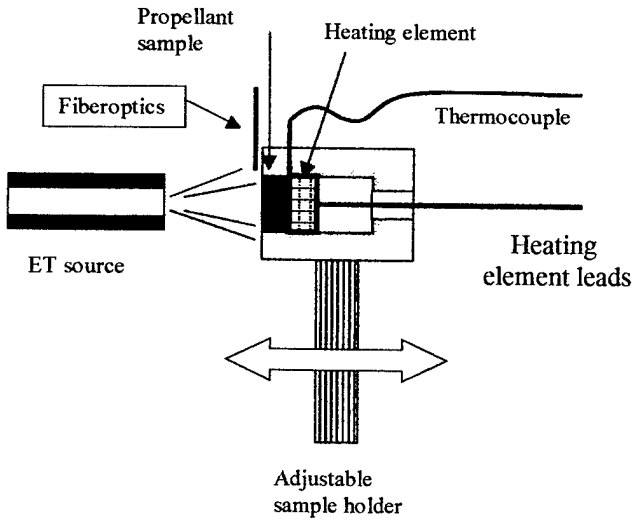

Fig. 8 Schematic of the experimental setup using heating a heating element to elevate the bed's temperature prior to plasma injection on the propellant sample

The sample holder is tube-shaped and has a seat for the propellant sample, which resides on the heating element. The temperature of the back surface of the propellant is monitored via a thermocouple. The sample is thin, about 1-2mm and the sample temperature is kept stable to the desired temperature via the heating element controller. The holder has a fiberoptic cable to view the plasma at the plasma-propellant interface. The entire holder is adjustable and can be placed at any location on the axis of the

plasma source. Experiments are conducted at a base pressure of 20 Torr for extinguished burn (interrupted burn) such that the burn is only during the plasma pulse length (100 μs discharge). The initial and final weights of the propellant sample are recorded, as well as the initial and final weights of the plasma source liner and the source electrode. For each shot, the discharge current is fed to our TITAN 2-D code [28] to calculate the plasma exit parameters. Plasma temperature at the plasma-propellant interface is calculated from optical emission spectroscopy measurements using copper lines.

A block diagram of the experimental arrangement is shown in Fig. 9, where PIPE represents the ETC experimental facility powered by a 360μF, 10kV high energy-density capacitor. The block diagram shows experimental components and data acquisition system, thermocouples and fiber optics to optical multichannel analyzer.

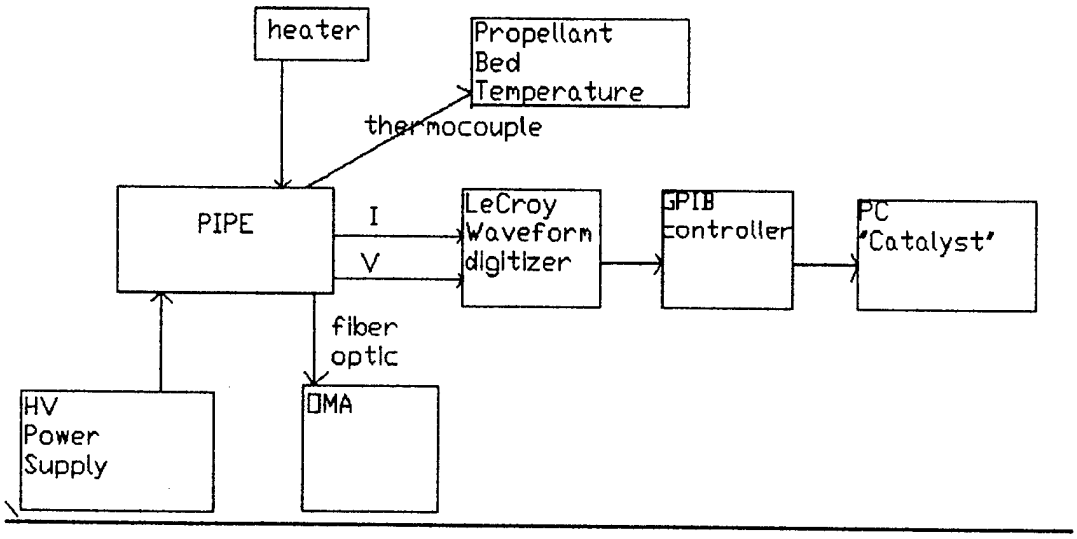

Fig. 9 Block diagram of the experimental setup for temperature sensitivity measurements

The sample holder was designed, essentially, to be a rectangular block with supporting rods that could be bolted to the bottom of the ETC chamber of the PIPE facility. The heater used was a 3/8″ diameter OMEGA cylindrical cartridge heater that was placed on a shelf and held in place by an aluminum plate. A small copper tube was attached to the holder by epoxy in order to keep the propellant sample from sliding against the pressure and provides a way to maintain thermal contact. The initial temperature of the propellant bed was monitored by a thermocouple pressed against the exposed face facing the plasma. The original method for controlling the heater output was an Omega Process Controller that controls the heater temperature using an output relay. This controller was chosen because it would keep the heater temperature essentially constant, and could be monitored and controlled through varying the voltage across the heater. However, two units were destroyed in a relatively short time because of the high-voltage high-current discharge. A large potentiometer was

added to the system and used to power the heater. The potentiometer regulates the voltage on the heater at a given time, thus controlling the current and temperature of the heater. This setup required careful monitoring of the rate of temperature increase so that the experiment would be performed at the time corresponding to the desired propellant bed temperature. It was possible to obtain a pseudo-steady state temperature with this device after an hour and a half of operation because the heat losses to the environment would eventually balance out the input heat flux to the heater.

III.2 Bed Temperature Sensitivity Results

Results of the propellant bed's temperature sensitivity have shown an increasing burn rates with increased bed temperature. For the variation of bed temperature between 23 to 50°C, the best fit is showing a power law of the form: Burn rate $BR = A_1 T^m$, where the burn rate is measured by dividing the interrupted erosive thickness by the plasma impact time (FWHM). Here in this equation, T is the bed temperature in °C, A_1 is proportionality constant and m is the power exponent. This equation can be introduced to the burn rate equation such that the burn rate, including bed temperature, may be expressed by: $BR = A P^a T^b$, where the first term (P^a) represents the conventional equation for the burn rate without introducing the bed's temperature. A more general equation may be introduced as: $BR = A P^a (T/ T_{ambient})^b$, and thus for $T = T_{ambient}$, the burn rate falls to the known equation. Bearing in mind that the pressure exponent 'a' with plasma ignition is much higher than its value for conventional ignition. The following graph shows the experimental results for elevated temperature regime with the propellant situated 2 inches from the source exit. When the propellant is closer to the source exit, it is expected that the burn rate will be much higher because of the pressure effect (momentum effect) on the burn rate.

When expressing the burn rate by the equation Burn Rate $BR = A P^{\alpha}$, it has been shown for JA-2 that the burn rate in conventional ignition is given by $BR = 203.2 \times 10^{-5} P^{0.889}$, while for plasma ignition it was shown to have a higher exponent: $BR = 8.865 \times 10^{-5} P^{1.376}$. As stated above, to include the effect of the bed temperature, it is necessary to modify the burn rate equation to include the bed temperature $BR (P,T) = a P^b f(T) = a P^b T^c$, where T is the bed temperature. The burn rate may be expressed in terms of normalized bed temperature in the form

$$BR = a P^b \left(\frac{T}{T_o} \right)^c$$

Where To represents the ambient (room) temperature. This model is more convenient to relate the burn rate to the ratio between elevated temperature to ambient temperature, or could be expressed as the burn rate change for a percentage change in the bed temperature. The advantage of this model is that it directly reduces to the Saint Roberts burn rate at ambient temperature. Figure 10 shows experimental results obtained for JA-2 burn rates versus increased bed temperature for one data set at 2-inches from the electrothermal source exit. It is obvious that the data easily fits a power law with a 2.4767 exponent.

The burn rate data for all selected axial locations of 1, 2 and 2.75 inches are shown in Fig. 11 as a function of the normalized temperature (T/T_o). The burn rate data shows that the 1-inch shots have the

highest burn rate and the 2-inch the lowest. Initially one may think that the 2.75-inch data should be the lowest and these data are in error. However, referring to the pressure data obtained by the compact multi-head probe as previously shown in section II, it is shown that total plasma pressure actually increases slightly between 2 and 3 inches as a result of momentum transfer and expansion.

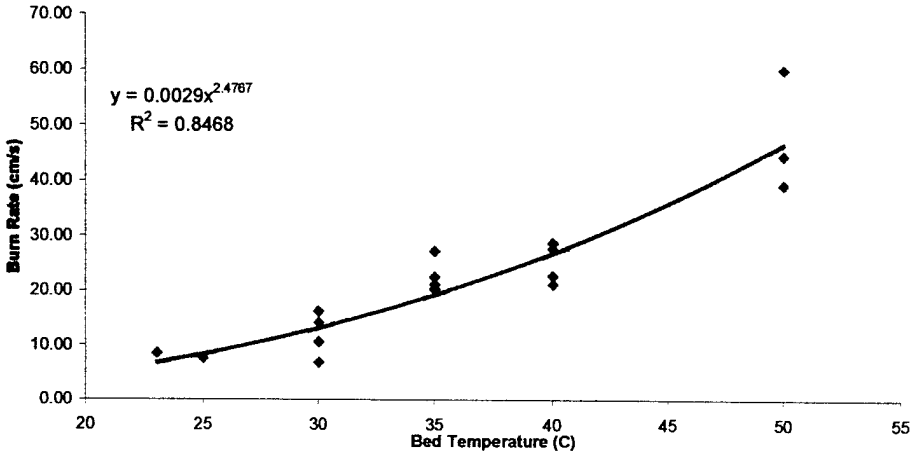

Fig. 10 Burn rate of JA-2 with increased bed temperature. Sample placed 2 inches from the exit of the ET source. Data fit to power law with 2.4767 temperature exponent

Since the pressure of these data was not directly measured, a method of evaluating the pressure is to compare the source exit pressure with previously measured pressures. The plasma diagnostic code TITAN was run to determine the barrel exit pressure at atmospheric conditions and then this value was fitted to the values obtained by compact probe measurements (as previously described in section II). TITAN is a pseudo 2-D code that calculates the plasma parameters at the source exit both spatially and as a function of time. TITAN was also used with base pressure of 20 Torr (the experimental conditions) and compared to compact probe results to see if the chamber pressure had any significant effect on plasma pressure. TITAN revealed that there is no significant change between the plasma expanding at 20 Torr or expanding at 760 Torr [6]. The plasma barrel pressure was approximately 11,400 psi independent of the initial chamber pressure. This value was fitted to compact probe data at 2,3, and 4 inches to approximate the plasma pressure at corresponding distances. The pressure values are shown in Table 1 below.

Table 1: Plasma Pressure (Total)

Distance (inches)	Pressure (psia)
1	1403.6
2	295
3	304

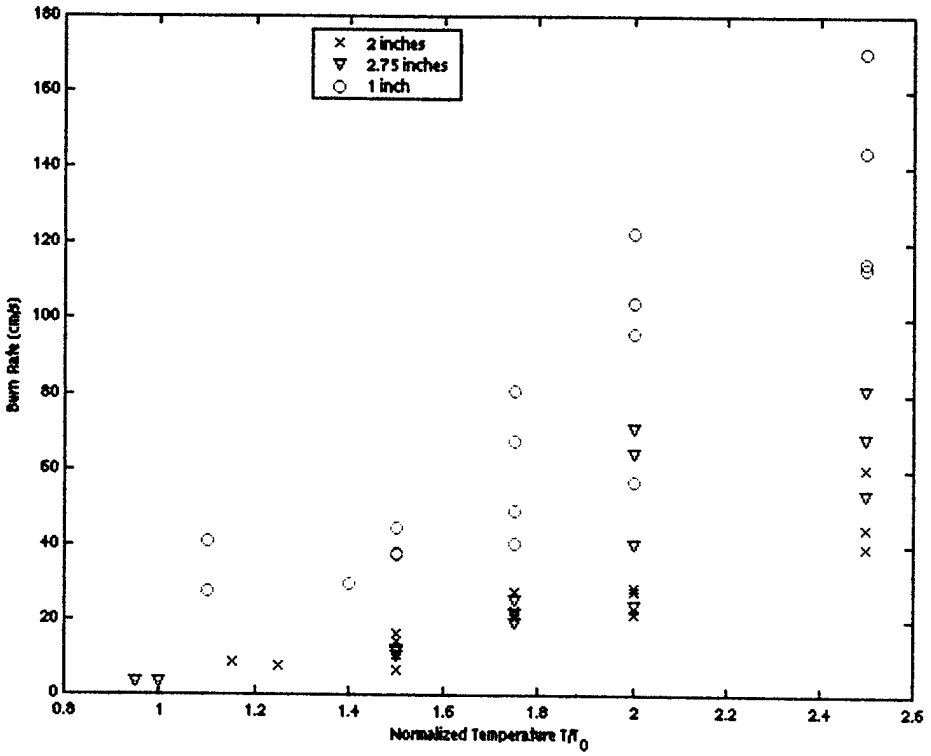

Fig. 11 Burn rate of JA-2 with increased bed temperature for all samples' positions. Normalized temperature (T/T_o) is used in this graph

Matlab's nonlinear least squares function, lsqnonlin, was used to determine the unknowns in the modified burn rate equation with values shown in Table 2.

$$BR = a\,P^{b}\left(\frac{T}{T_o}\right)^{c}$$

Table 2: Exponents and constant, a, of burn rate equation

Parameter	Value
a	0.355
b	0.528
c	2.362

Thus, the modified burn rate equation may be written as:

$$BR = 0.355P^{0.528}\left(\frac{T}{T_o}\right)_{JA2}^{2.36}$$

This equation fits well the data set obtained at all measured locations, as seen in Fig. 12.

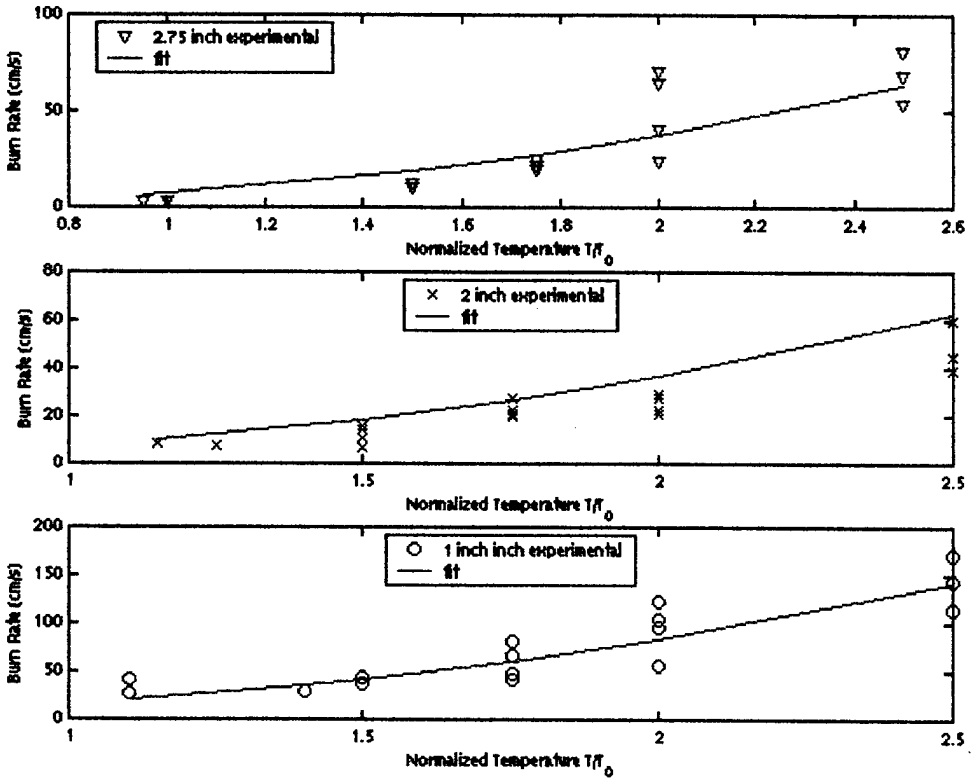

Fig. 12 Burn rate of JA-2 with increased bed temperature for all samples' positions. Normalized temperature (T/T_o) is used in this graph. Data fitting used normalized burn rate equation.

However, it can be seen that the 2-inch data is not well fitted. This indicates there is another factor that is not taken into account in the above equation. The equation should reduce to the numbers obtained by Zaghloul et al [5] when the propellant bed reaches ambient temperature. This was not the case. The burn rates obtained in this experiment at propellant ambient temperatures were much higher than those obtained previously at similar pressures. The difference is attributed to the way the nonlinear solver fits the function. A quick calculation at 11,400 psi and propellant bed at ambient still shows an increased burn rate with plasma injection over conventional means. With plasma injection the burn rate at ambient temperature is 49.2 cm/sec verses 8.2 cm/sec for conventional ignition. The equation obtained by Zaghloul et al [5] yields a burn rate of 33.72 cm/sec with plasma injection. In general, the new modified form follows the same trend even though the pressure exponent is not as large.

This is due to the large difference in the magnitude of the constant 'a' and the pressure range looked at. The equation in this form does provide a good application oriented equation because impact pressure is a common measurable value in cannon ballistics. It is also possible to remove the pressure dependence by taking the ratios of the burn rates at a raised bed temperature to the burn rate at ambient bed temperature. Thus, the equation may then be written as:

$$\frac{(BR)_T}{(BR)_{T_o}} = \frac{aP^b T^\gamma}{aP^b T_o^\gamma} = C\left(\frac{T}{T_o}\right)^\gamma_{JA2}$$

where C is a constant. This equation is valid for other ignition means, e.g. conventional or laser, because it depends only on the propellant bed temperature.

Each burn rate data set was analyzed and was normalized to the ambient propellant burn rate. The values used for the normalization were the burn rates at T=20°C or the average of the coolest ambient data point available. The 1-inch data was normalized to 34.325, 2 inches to 8.566, and 2.75 inches to 3.485 cm/sec. Normalized burn rate is shown in Fig. 13.

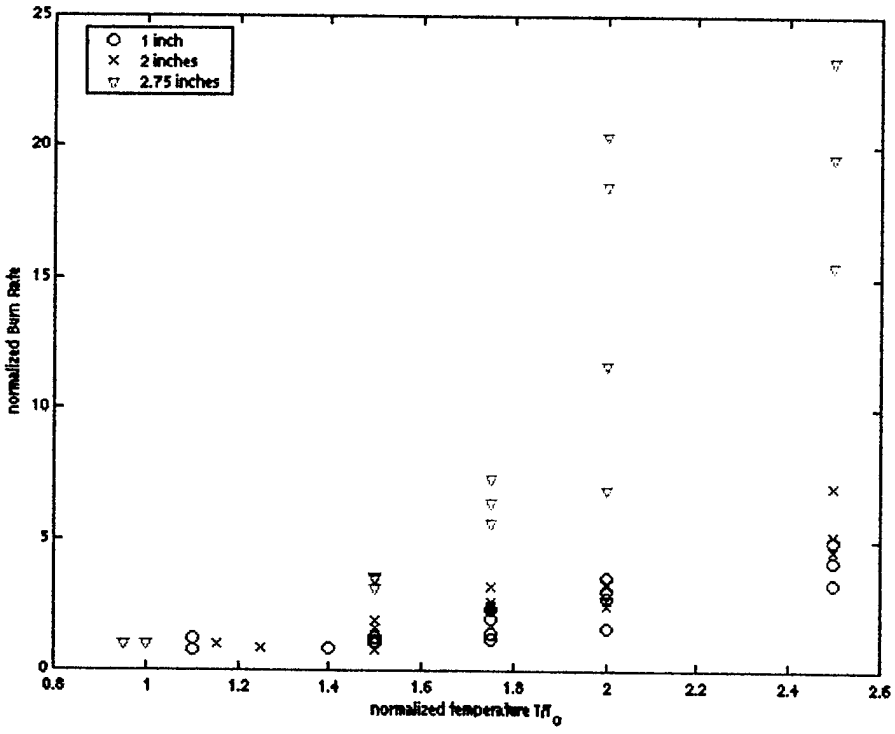

Fig. 13 Normalized burn rate of JA-2 with increased bed temperature for all samples' positions.

It can be seen from Fig. 13 that the normalized burn rates at 1 and 2 inches are almost the same while the normalized burn rate at 2.75 inches increases significantly.

The normalized equation was transformed into a log form and a linear fit was performed.

$$\ln\left(\frac{(BR)_T}{(BR)_{T_0}}\right) = \ln(C) + \gamma \ln\left(\frac{T}{T_0}\right)_{JA2}$$

The fit parameters are shown in Table 3 for 1, 2, and 2.75 inches from the electrothermal source exit.

Table 3: Temperature Exponent γ and constant C for 1, 2 and 2.75 inches

	C	γ
1-inch	0.6110	1.9721
2-inches	0.5638	2.4767
2.75-inches	1.0352	3.3312

These fits are shown in Figures 14, 15 and 16.

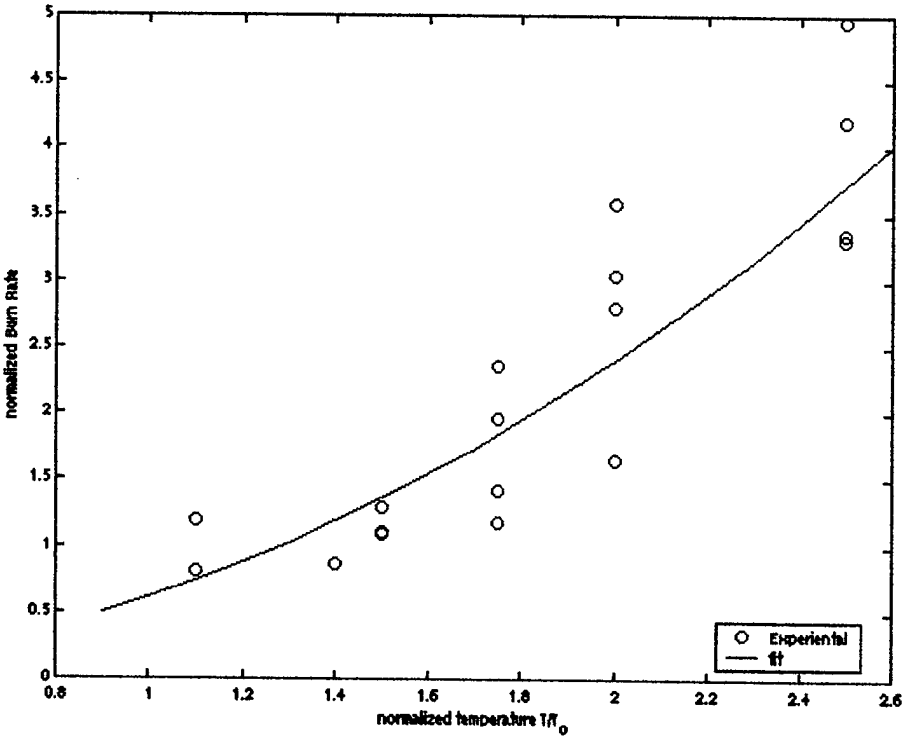

Fig. 14 Normalized Burn Rate Fit for d=1 inch from the source exit

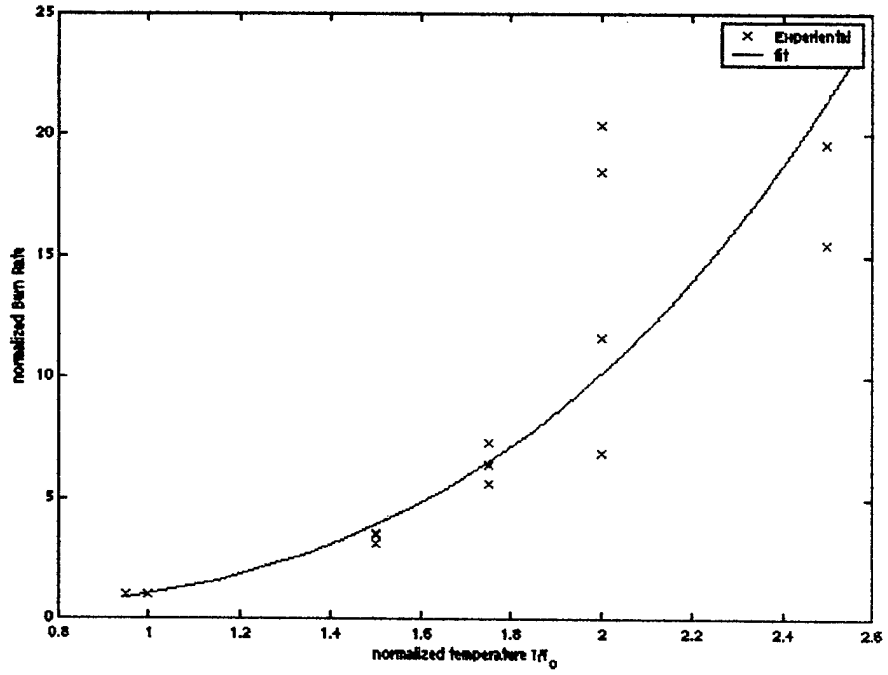

Fig. 15 Normalized Burn Rate Fit for d=2 inch from the source exit

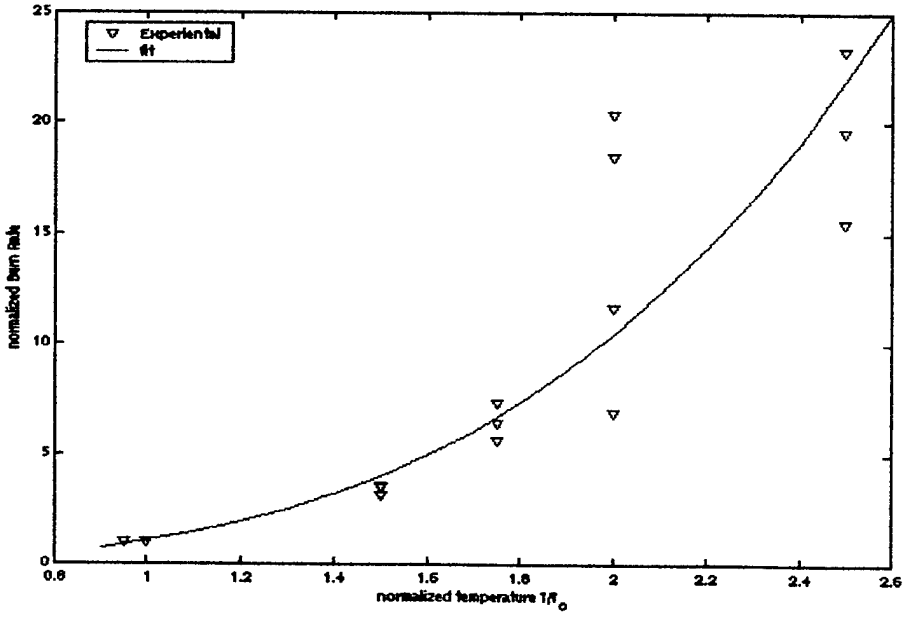

Fig. 16 Normalized Burn Rate Fit for d=2.75 inch from the source exit

These figures show that the propellant bed temperature augments the data more the farther it extends beyond the barrel, which indicates the burn rate is also dependent on the distance from the source. The conclusion here is that the plasma parameters do play an important role in propellant burn

and need to be incorporated into the equations. An additional functional form, with dependence on bed temperature and distance from the source section is proposed.

$$\frac{BR}{BR_o} = C\left(\frac{T}{T_o}\right)_{JA2}^{b}\left(\frac{d}{d_o}\right)^{\gamma}$$

where the naught values are taken at an arbitrary distance from the source.

Since $P = \Sigma\, nkT_p$, the pressure may then be substituted in the burn rate equation to include plasma parameters in lieu of the pressure:

$$BR = a(nkT_p)^{b}\left(\frac{T}{T_o}\right)_{JA2}^{\gamma}$$

where n is the plasma density, k is the Boltzmann constant, and T_p is the plasma temperature.

Plasma temperature can be related to plasma heat flux utilizing the Blackbody assumption such that the plasma temperature could be expressed in terms of the blackbody heat flux q'':

$$T = \left(\frac{q''}{\varepsilon\sigma}\right)^{\frac{1}{4}}$$

where ε is the emissivity and σ is the Stefan-Boltzmann constant. For simplicity, the emissivity ε is assumed to be equal to 1, and thus, substituting for the plasma temperature yields an expression for the burn rate in terms of radiation heat flux:

$$BR = An^{b}\left(\frac{T}{T_o}\right)^{\gamma}(q'')^{\frac{b}{4}}$$

where A is a constant.

Optical emission spectroscopy has been performed to determine the plasma temperature and density. Copper lines were used to obtain plasma temperature and number density. The lines used for the temperature analysis and their parameters are shown in Table 4.

Table 4: Copper lines used for Spectroscopic Analysis

Spectrum	Wavelength (nm)	E_i (eV)	gA ($10^8 s^{-1}$)
Cu I	510.554	3.82	0.080
Cu I	515.324	6.19	2.4
Cu I	521.820	6.19	4.5
Cu I	529.250	7.74	0.436
Cu I	570.020	3.82	0.0096
Cu I	578.213	3.79	0.033

Three spectral samples are shown for each distance in Figures 17, 18 and 19, to demonstrate reproducibility of the spectral data, thus indicating similar properties.

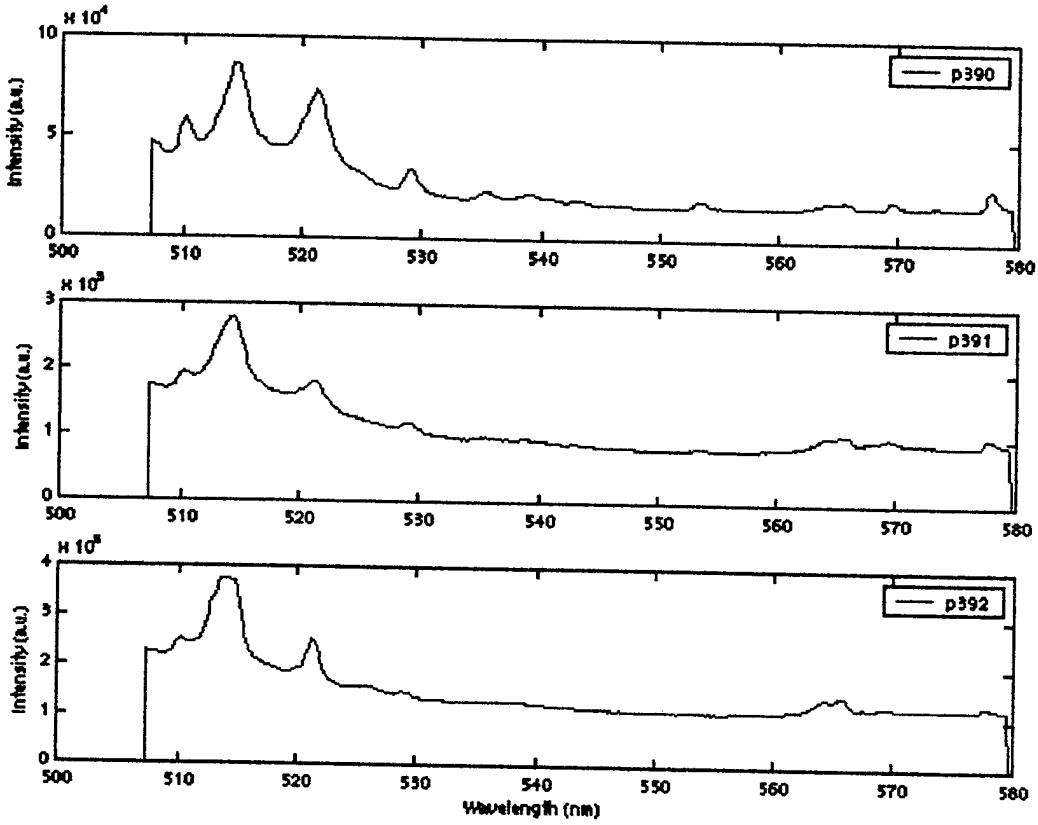

Fig. 17 Sample three d = 1-inch shot Spectra

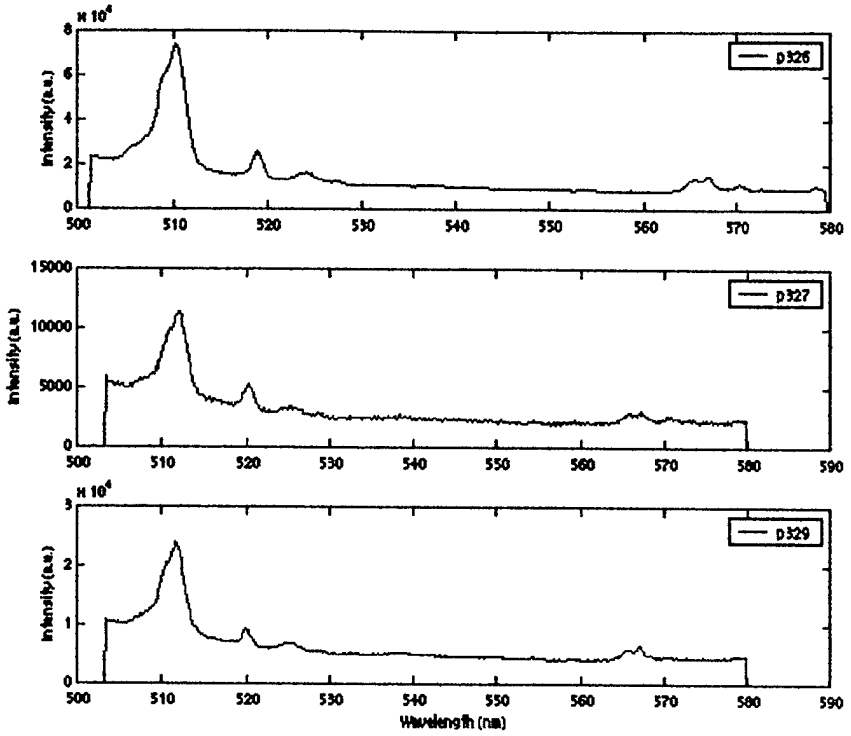

Fig. 18 Sample three d = 2-inch shot Spectra

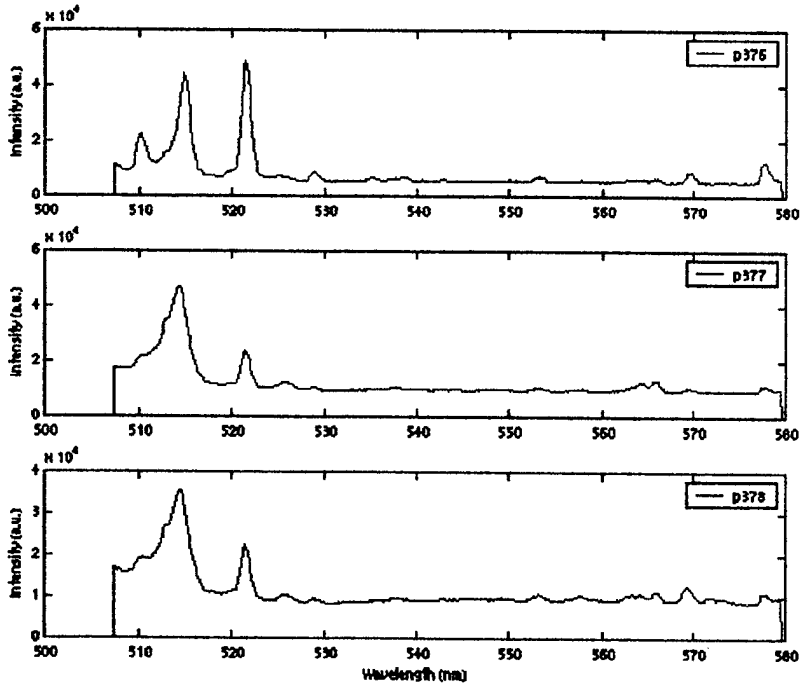

Fig. 19 Sample three d = 2.75-inch shot Spectra

The PEAKFIT [29] program was used to determine all measured peaks in the spectra. It can determine all the peaks, obvious and hidden, and outputs them and their areas to file for analysis. Table 5 shows plasma temperature, density and the corresponding radiation heat flux at the three locations 1, 2 and 2.75 inches from the source exit.

Table5: Average Plasma Temperature, Heat Flux, and Density

Distance (in)	Temperature (eV)	Heat Flux $*10^8$ W/m^2	Density $*10^{24}$ m^{-3}
1	0.846	5.237	3.575
2	0.687	2.289	3.406
2.75	0.821	4.666	2.614

The purpose for determining these temperatures is to attempt to determine the burn rate dependence on plasma parameters as well as propellant bed temperature. A burn rate ratio can be determined between the distances that will allow correlation with number density and plasma heat flux. The ratio can be expressed as:

$$\frac{(BR)}{(BR)_o} = A\left(\frac{n}{n_0}\right)^b \left(\frac{q''}{q_o''}\right)^{\frac{b}{4}} \left(\frac{T}{T_o}\right)_{JA2}^{\gamma}$$

The only question about this equation is what the normalizing condition should be. The reasonable choice is the plasma density because it dominates the plasma temperature in the kinetic pressure term $P = \Sigma\, nkT$. For this reason, all naught values are those of the 2.75 inch data at ambient temperature so that the burn rate ratio would reduce to one at that point. Utilizing the values obtained for plasma temperature and density allows the unknowns of the above equation to be determined using Matlab's nonlinsq function and are shown in Table 6.

Table 6: Parameters of the modified equation with dependence on plasma radiation heat flux and number density, and the normalized bed temperature with respect to ambient

Parameter	Value
A	1.8315
b	2.6114
γ	2.8365

Hence, the burn rate equation can now be written as:

$$\frac{(BR)}{(BR)_o} = 1.8315\left(\frac{n}{n_0}\right)^{2.6114} \left(\frac{q''}{q_o''}\right)^{0.6529} \left(\frac{T}{T_o}\right)_{JA2}^{2.8365}$$

This Equation provides an insight into the effect of plasma density and radiation heat flux on the burn rate of the propellant bed. It is now possible to predict burn rate augmentations based on the plasma density and heat flux variations as well as propellant bed temperature.

IV. Arc Channels

IV.1 Arc Channel Experiment

Experimental arrangement to initiate an arc channel in a propellant sample was arranged using a high voltage pulsing device. Such arcs generated by HV pulsers are usually easy to generate at atmospheric conditions. The arc may take any shape from one pulse to another depending on the triggering circuitry and the atmospheric conditions during the time of measurements. However, with short arcs generated between thin electrodes at small separating distance, consistency of the arc parameters could be obtained. Figure 20 shows the experimental arrangement of developing an arc channel in a propellant sample. The sample is situated between two electrodes to the output of a high voltage pulser. The pulser may be triggered once or multiple pulses may be produced at a selected repetition rate.

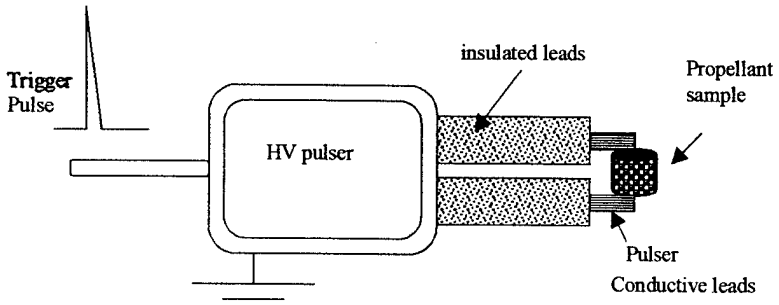

Fig. 20 Experimental arrangement to develop an arc channel in a propellant sample at atmospheric conditions. Single or multiple pulses may be produced.

The propellant sample resides between the pulser leads such that the arc is initiated through the central perforation of the JA-2 sample. This will initiate the arc with its core inside the propellant as illustrated in Fig. 21(A), where the arc core joule-heats the inner wall of the propellant. Also, an exploding wire may be inserted in the central perforation, Fig. 21(B) and connected to the pulser to initiate the arc via wire explosion.

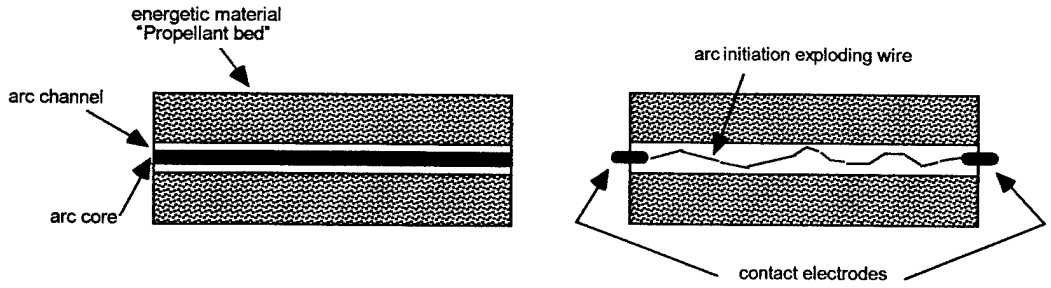

Fig. 21 Arc initiation inside the central perforation (A), and by fuse-operated arc (B) inside the central perforation of a propellant sample.

The arc voltage can be increased to up to 30kV with arc current up to 70A, and pulse length of approximately 10-20 ns, giving rise to arc energies of several of mJ. Typical arc current has a peak of about 1.0 A at a peak discharge voltage of 12kV for most experiments. The integrated energy of a typical arc is less than 120 mJ, which makes it perfect to simulate the mJ energy range of arc channels

developing in a propellant bed. Controlling the arc energy in the present pulser is via the arc voltage, which provides a wide range of arc energy between few milli-joules to several joules. The arc current is sharp enough to closely simulate initiation of narrow arc channels at considerably short period of time. The arc current is measured by a Pearson coil and arc voltage is measured by a compensated capacitively-coupled high voltage probe. Figure 22 shows a schematic of the experimental arrangement for milli-joule to several joules arc discharge.

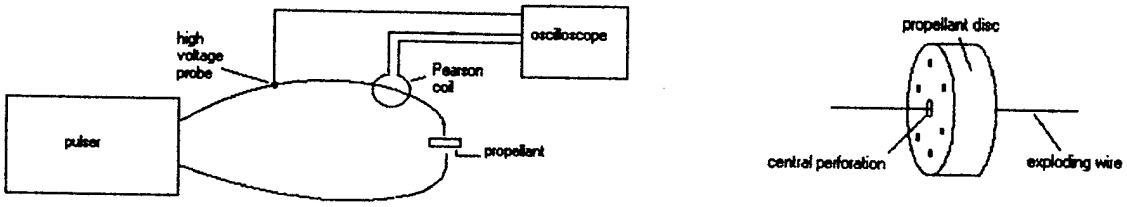

Fig. 22 Schematic of experimental arrangement for low-energy arc channels in solid propellant sample.

Experimental data have shown a weight change of ±0.03 mg for such low-energy arcs, which prompts the need to either increase the arc energy or to pre-stress the sample by compression. The choice of increasing arc energy has been chosen to investigate effect of arc energy on initiation threshold. Arc energy between 260 and 1050 joules were used and the corresponding mass loss was measured. Figure 23 shows experimental mass loss data versus arc energy, and a linear fit to experimental data. The linear fit $\Delta m = 2 \times 10^{-4} (E + 282)$, where Δm is the mass loss in mg and E is the arc energy in joules. The linear fit has $R^2 = 0.8917$, almost 0.9. This medium-range arc energy shows an increased erosive burn with increased energy of the arc, and it is consistent with previous results of plasma enhanced burn rates of same propellant [4,5].

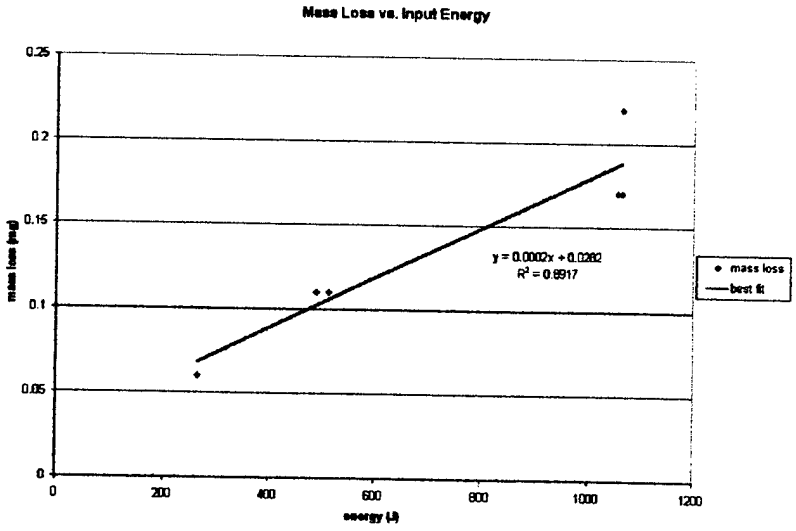

Fig. 23 Measured weight loss of propellant's sample versus arc energy showing increased burn rate with increased energy. The linear fit has $R^2 \sim 0.9$.

IV.2 Arc Channel Model

Arc channel may be modeled as a confined capillary discharge, which is similar to modeling electrothermal plasmas in ablation-controlled arc regime [11,14,28].

The electron-ion collision frequency is necessary to compute e-i momentum transfer. The Coulomb logarithm in such arc regime, with high density and low temperature, needs be modified and the approximation model proposed by Zollweg-Liebermann has formula [30] $\ln\Lambda = \ln\sqrt{1+1.4\Lambda_m^2}$, where the term Λ_m is a modified Coulomb parameter, and is equal to:

$$\Lambda_m = \frac{\sqrt{\lambda_D^2 + \lambda_+^2}}{\overline{b}_0}$$

Here λ_D is the Debye length (m), λ_+ is the mean ionic radius (m), and $\overline{b}_0$ is the average thermal impact parameter (m) for 90° scattering of incident electrons. The mean ionic radius is given by:

$$\lambda_+ = \left[\frac{4}{3}\pi\sum_{i=1}^{i_{max}} n_i\right]^{-\frac{1}{3}}$$

This summation is taken over all possible ionization states (n_i is the number density of ionization state i), including neutrals (represented by $i = 1$). Consequently, the electron-ion collision frequency, including the modified Coulomb logarithm, will be given by [28,30]:

$$\overline{\nu}_{ei} = \frac{38 Z_{eff} n_e e^2 \ln\sqrt{1+1.4\Lambda_m^2}}{\gamma_e m_e T^{3/2}}$$

with Z_{eff} is the effective charge state of the plasma, γ_e is the correction factor for e-e collisions, and m_e is the rest mass of the electron. The conductivity of the plasma 'arc' is finally given by:

$$\sigma = \frac{n_e e^2}{m_e}\left(n_0 \overline{Q}_{e0}\sqrt{\frac{8kT}{\pi m_e}} + \overline{\nu}_{ei}\right)^{-1}$$

Here $\overline{Q}_{e0}$ is the momentum transfer cross section for electron-neutral collisions. The conductivity directly influences the volumetric heating of the plasma, which is assumed to be composed only of Joule heating:

$$q''' = \frac{J^2}{\sigma}$$

J is the magnitude of the vector quantity of the current density (A/m^2), and σ is the plasma conductivity (S/m). This volumetric heat generation rate (W/m^3) then goes into the energy equation, which is coupled to the momentum and continuity equations. They are given below, in the order of energy, momentum, and then continuity:

$$\frac{\partial(\rho u)}{\partial t} + \nabla\cdot(\rho u\vec{v}) = -P\nabla\cdot\vec{v} + \nabla\cdot\lambda\nabla T + q'''$$

$$\frac{\partial(\rho\vec{v})}{\partial t} + \nabla\cdot(\rho v\vec{v}) = -\nabla P + \nabla\cdot\vec{\sigma}_z + \vec{J}\times\vec{B}$$

$$\frac{\partial \rho}{\partial t} + \nabla \cdot (\rho \vec{v}) = 0$$

A number of variables are introduced here. Thermodynamic variables include the pressure (Pa), temperature (K), specific internal energy (J/kg), and physical density (kg/m^3), which are P, T, u, and ρ, respectively. Flow variables include the velocity (m/s), conductivity (sum of thermal and radiative conductivities, W/m · K), and shear stress (N/m^2), given as $\vec{v}$, λ, and $\vec{\sigma}_z$, respectively. Finally, the electromagnetic terms are the current density (A/m^2) and magnetic field strength (T), given as $\vec{J}$ and $\vec{B}$, respectively [28]. The code results, for an assumed flat-top arc current over a 50 μs period, inside a polycarbonate tube that simulates central perforation of a propellant have shown higher temperatures than observed ones. Figure 24 shows the temporal plasma arc temperature as calculated by the code. It is suggested that the approximation of the Coulomb logarithm is not accurate and results in over-estimation of the plasma arc temperature. The code results for aluminum capillary, simulating fuse operation, is shown in Fig. 25, where the temperature peaks to almost same value as that of polycarbonate. The difference is in the faster temperature decay for the aluminum case, due to heat conduction to the channel wall. However, it is over-predicting the temperature. A modification to the Coulomb logarithm should be introduced to account for plasma non-ideality with better approximation or a complete non-approximated solution. This modification will be investigated in a future phase.

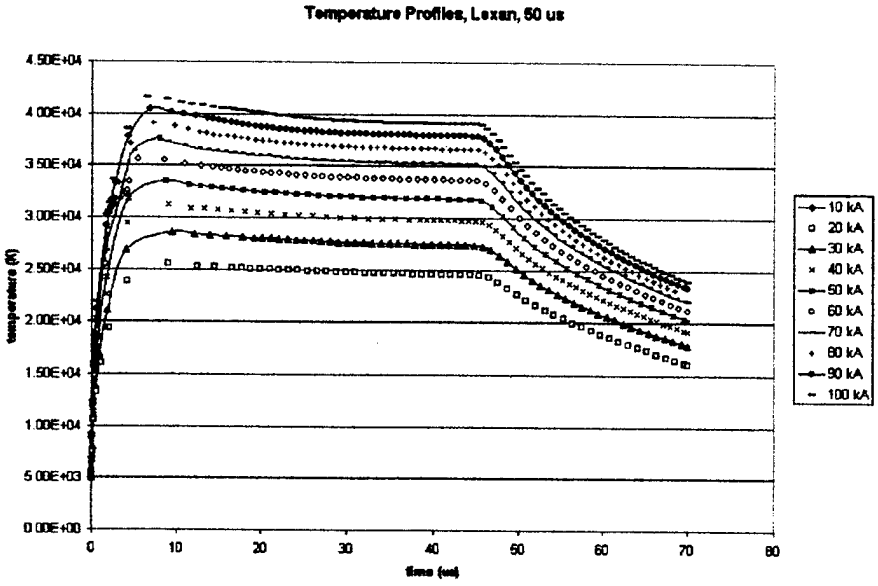

Fig. 24 Calculated plasma arc temperature, in a polycarbonate capillary tube, as a function of time for a flat-top current profile.

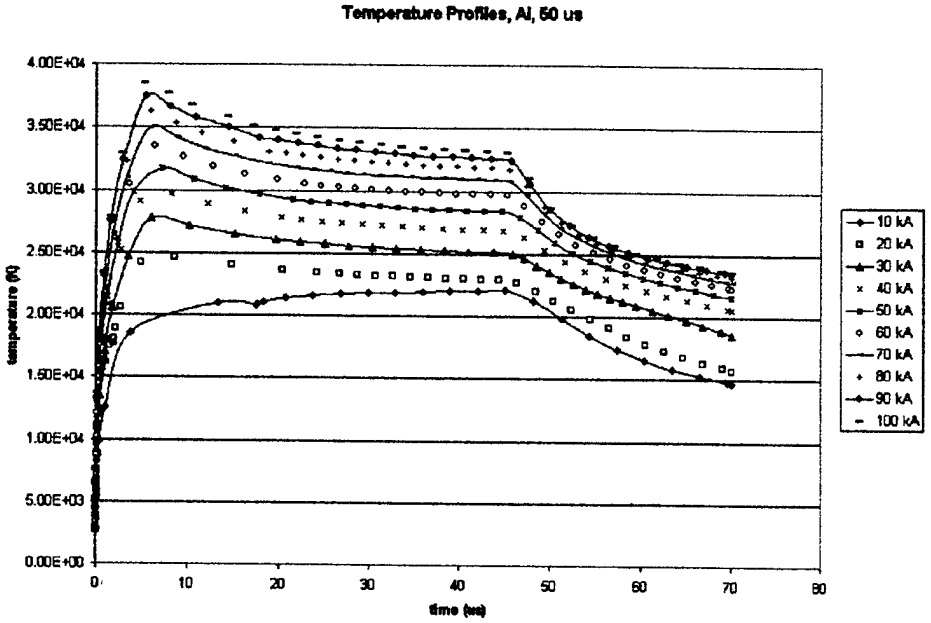

Fig. 25 Calculated plasma arc temperature for an aluminum capillary, simulating aluminum fuse, as a function of time for a flat-top current profile.

V. Conclusion

The plasma flow-field parameters were measured showing the distribution of essential parameters, such as pressure, temperature, number density and average speed. The importance of such plasma-flow-field characterization is to help in the design of electrothermal-chemical devices by knowing the distribution of the plasma jet parameters.

It is concluded that there is a power law burn rate dependence on propellant bed's temperature. This has been shown experimentally and has a reasonable physical meaning because of the extra energy given to the propellant bed due to the heat energy input. The functional form of burn rate equation has been expressed in various forms but always includes the bed's temperature. A useful form is that of the normalized bed temperature with respect to ambient temperature and a dependence on the pressure. Another form is the ratio form between burn rates at elevated temperature to that at ambient. The form that includes plasma parameters in terms either of plasma temperature or radiation heat flux is of more importance in order to characterize effect of plasma augmentation mechanism on burn rates.

Arc modeling, using approximation to the Coulomb logarithm, has shjown over-prediction of the plasma arc temperature. This over-prediction has been proven for the case of polycarbonate and aluminum. The approximation affects the calculation of the electron-ion collision frequency and consequently the plasma arc conductivity, which directly affects the joule heating term in the energy equation. A better approximation of the modified Coulomb logarithm, or a complete non-approximated form should be introduced to account for plasma non-ideality, which will be investigated in a future phase.

VI. References

[1] L.E. Harris, et al. "Enhanced propellant burn rate through plasma erosion," Proc. 30th JANNAF Combustion Meeting, CPIA Publication 606, vol. IV, pp.121-135, November 1993.

[2] M.A. Bourham, J.G. Gilligan, C.D. Buchanan and C.F. Boyer, "Effect of Electrothermal Plasma Parameters on the Burn Rates of JA-2 Solid Propellant for ETC Guns", Proc. 33rd JANNAF Combustion Meeting, Monterey, CA, 4-8 November 1996, CPIA Publication 653, Vol.I, pp. 57-66, 1996.

[3] C.R. Woodly and S. Fuller, "Apparent Enhanced Burn Rates of Solid Propellants due to Plasmas", Proc. 16th International Symposium on Ballistics, San Francisco, CA, 23-28 September 1996, Vol.1, pp.153-160, 1996.

[4] M.A. Bourham, J.G. Gilligan and W.F. Oberle, "Analysis of Solid Propellant Combustion Behavior Under Electrothermal Plasma Injection for ETC Launchers", IEEE Trans. Magnetics, Vol. 33, pp.278-283, January 1997.

[5] Mofreh R Zaghloul, Krupakar S.Murali, John G. Gilligan, Orlando E. Hankins and Mohamed A Bourham, "Analysis and Experimental Studies of Plasma-Propellant Interaction and Effect of Plasma Parameters on Burn Rates of JA2 Solid Propellant for ETC Guns," 35th JAANAF Combustion Subcommittee Meeting, Tuscson, AZ, 7-11 December 1998, CPIA Pub. #680, Vol. I, pp. 247-257, December 1998.

[6] Subramanian K. Murali, "Optical Emission Spectroscopy of electrothermal Plasmas and Verification of Local thermodynamic Equilibrium." MS Thesis, NCSU, 1998

[7] Richard A Beyer, "Small Scale Experiments in Plasma-Propellant Interactions," 37th JANNAF Combustion Subcommittee Meeting, Monterey, CA, November 2000, CPIA Pub. #701, pp. 137-144, November 2000.

[8] Avi Birk, Miguel Del Guercio, Amy Kinkennon, Douglas E. Kooker and Pamela Kaste, "ETC Closed-Chamber Interrupted-Burning Tests with JA2 and M30 Solid Propellants," Weapons and Materials Research Directorate, Army Research Laboratory, Aberdeen Proving Ground, MD, 21005-5066 October 1999.

[9] C. Edwards, M. Bourham and J. Gilligan, "Operational Characteristics and Preliminary Results of a Plasma-Propellant Interaction Experiment", Proc. 30th JANNAF Combustion Meeting, CA, 15-19 November 1993, CPIA Publication 606, Vol.I, pp.27-32, November 1993.

[10] C.M. Edwards, M.A. Bourham and J.G. Gilligan, "Experimental Studies of the Plasma-Propellant Interface for Electrothermal-Chemical Launchers", IEEE Trans. Magnetics, Vol. 31, pp.404-409, January 1995.

[11] A. Loeb and Z. Kaplan, "A Theoretical Model for the Physical Processes in the Confined High Pressure Discharges of Electrothermal Launchers", IEEE Trans. on Magnetics, Vol. 25, No.1, 342, January 1989.

[12] J. Batteh, J. Powell, D. Sink and L. Thornhill, "A Methodology for Computing Thermodynamic and Transport Properties of Plasma Mixtures in ETC Injectors," IEEE Trans. Magnetics, vol. 31, p.388, January 1995.

[13] M. Nusca and K. White, "Plasma Radiative and Convective Interactions with Propellant Beds", Proc. 34th JANNAF Combustion Meeting, Monterey, CA, 4-8 November 1996, CPIA Publication 662, Vol.I, pp. 21-33, 1997.

[14] R.B. Mohanti, J.G. Gilligan and M.A. Bourham, "Time Dependent Simulation of Weakly Nonideal Plasmas in Electrothermal Launchers", Physics of Fluids B "plasma physics", Vol. 3, No. 11, 3046, November 1991.

[15] R.J. Lieb and C.J. Gillich, "Morphology of Extinguished Monolithic JA2 Grains Fired in a 30-mm Solid Propellant Electrothermal-Chemical (SPETC) Gun," Army Research Laboratory, ARL-TR-606, November 1994.

[16] K. White, G. Katulka and S. Driesen, "Electro-Thermal Chemical Plasma Interaction with Propellants," Proc. 32nd JANNAF Combustion Meeting, NASA Marshall Space Flight Center, Huntsville, AL, CPIA Publications 631, Vol.1, pp.113-122, October 1995.

[17] J.R. Greig, J.R. Earnhart, N.K. Winsor, H.A. McElroy, A.A. Juhasz, G.P. Wren and W.F. Morrison, "Investigation of Plasma-Augmented Solid Propellant Interior Ballistic Process," IEEE Trans. Magnetics, vol. 29, p.555, January 1993.

[18] W.F. Oberle and G.P. Wren, "Methods for Determining Burning or Gas Generation Rates of Plasma-Augmented Propellants with Applications to Electrothermal-Chemical (ETC) Guns," IEEE Trans. Magnetics, vol. 31, p.435, January 1995.

[19] G.P. Wren, W.F. Oberle, N.K. Winsor and A. Hosangadi, "Spatial Effects of an Electrically Generated Plasma on the Interior Ballistics of Electrothermal-Chemical (ETC) Guns," IEEE Trans. Magnetics, vol. 31, p.457, January 1995.

[20] J. Batteh, J. Powell, D. Sink and L. Thornhill, "A Methodology for Computing Thermodynamic and Transport Properties of Plasma Mixtures in ETC Injectors," IEEE Trans. Magnetics, vol. 31, p.388, January 1995.

[21] M. Nusca and K. White, "Plasma Radiative and Convective Interactions with Propellant Beds", Proc. 34th JANNAF Combustion Meeting, Monterey, CA, 4-8 November 1996, CPIA Publication 662, Vol.I, pp. 21-33, 1997.

[22] Chomiak, Jerzy. Combustion A Study in Theory, Fact and Application , Gordan and Breach Science Publishers, 1990

Distribution List

ADDRESSEES	NUMBER OF COPIES
Dr. Judah M. Goldwasser Office of Naval Research Ballston Center Tower One 800 North Quincy Street Arlington, VA 22217-5660	2
Office of Naval Research Regional Office Atlanta 100 Alabama St. NW , Suite 4R15 Atlanta, GA 30303-3104	1
Naval Research Laboratory ATTN: Code 5227 4555 Overlook Avenue, SW Washington, DC 20375-5320	1
Defense Technical Information Center 8725 John J. Kingman Road, STE 0944 Fort Belvoir, VA 22060-6218	1
Dr. Mohamed A. Bourham North Carolina State University Department of Nuclear Engineering Raleigh, NC 27695-7909	2
Total printed copies of this document	**7**

[23] Christopher M Hobbs, "Temporal and Spatial Characterization of a Freely Expanding Electrothermal Plasma Jet." MS Thesis, NCSU, 2000

[24] O. Hankins, M. Bourham, J. Gilligan, J. Earnhart, "Visible Light Emission Measurements from a Dense Electrothermal Launcher Plasma", IEEE Trans. on Magnetics, Vol. 29, p.1158, January 1993.

[25] O.E. Hankins, M.A. Bourham and D. Mann, "Observation of Visible Light Emission From Interactions Between an Electrothermal Plasma and a Propellant", IEEE Trans. Magnetics, Vol. 33, pp. 295-298, January 1997.

[26] E.J. Clothiaux, "Spectroscopic Observations of an Arc-Plasma Accelerator", J. Quant. Spectrosc. Radiat. Transfer, Vol. 44, No. 5/6, 567, 1990.

[27] Ryan M. Davis, "Bed Temperature Sensitivity of Plasma Ignited Propellant" MNE Thesis, NCSU, 2001.

[28] H.H. Ngo, M.A. Bourham and J.M. Doster, "Heat and Current Transport in a Metal-Vapor Electrothermal Plasma Source for Electrothermal-Chemical Guns", will be presented in the 35th JANNAF Combustion Subcommittee Meeting, Tucson, AZ, 7 - 11 December 1998.

[29] PeakFit™ 4.0 for Windows, peak separation and analysis software, User's Manual, 1997.

[30] R. Zollweg and R. Lieberman, "Electrical Conductivity of Nonideal Plasmas", J. Applied Phys., Vol 62, No. 9, 1987.